Paper: ASAT-17-015-TH

17th International Conference on
AEROSPACE SCIENCES & AVIATION TECHNOLOGY,
ASAT - 17 – April 11 - 13, 2017, E-Mail: asat@mtc.edu.eg
Military Technical College, Kobry Elkobbah, Cairo, Egypt
Tel: +(202) 24025292 – 24036138, Fax: +(202) 22621908

Experimental and Numerical Study of Air Sweeping Over Bare Water Flat Area

{A. A. Aboulkasem, S. El- Shamarka, M. S. Hassan, A. G. Ibrahim}*

Abstract: The transport criterion of water from a flat surface through a stream of air was predicted by developing a two-dimensional model. A special experimental device was designed and built for this purpose. Numerical simulation of heat and mass transfer processes was carried out using CFD. The developed model consists of water on one side and a stream of air blown along its top surface aiming at the establishment of an air humidifier. The operating conditions of this humidifier are adjusted to fulfill an adiabatic saturation process (air washer). The model uses the basic equations of momentum, heat, and mass balance. Computational runs were conducted using COMSOL Multiphysics® software. Experimental results showed good agreement with both computational CFD and analytical Psychrometry. The device performance proved sustainable and was used to study the effect of different conditions.

Keywords: Mass transfer, humidification, diffusion mechanisms, COMSOL Multiphysics®.

Nomenclature

c	concentration (mol/m^3)
C_p	heat capacity at constant pressure (J/(kg K))
D	molecular diffusion coefficient of water into air (m^2/s)
h	specific enthalpy (kJ/kg)
k	thermal conductivity (W/(m K))
P	total pressure (Pa)
R	gas constant (J/(mol K))
T	temperature (K)
u	velocity component in x-direction (m/s)
V	volume allowed for air-water mixing (m^3)
v	velocity component in y-direction (m/s)
W	humidity ratio (g water vapor/kg dry air)

Greek letters

ϕ	relative humidity (-)
ρ	fluid density (kg/m^3)
μ	viscosity (Pa s)

Subscripts

a	air
atm	atmospheric
in	inlet
out	outlet
sat	saturation
w	water
0	air inlet boundary

* Egyptian Armed Forces, Egypt.

1. Introduction

Concentration gradient in mixtures and compounds, let components diffuse in a direction which will decrease or eliminate the differences. Diffusion in fluids is often much greater in gases (around 10^{-4} m^2/s) compared to liquids (around 10^{-9} m^2/s). Mass transfer also occurs when a fluid is mixed; larger segments of the fluid are moved in different speeds and directions causing mass to mix. In all cases diffusion still occur but is no longer the main reason for transporting the components [1], [2].

Film theory, assumes that the mass and heat transfer between two phases, such as liquid-liquid, gas-liquid or liquid-solid, occurs through a stagnant film that exist perpendicular to the boundary surface. The stagnant films are present at both side of the interface and in that film only diffusion occurs. The velocity of the surrounding fluid does not affect what happens inside the film but it affects its thickness [3].

When a mass transfer leads to a phase transition, such as evaporation or condensation, heat is transferred as well. The heat loss or gain at the surface determines the direction of the heat transport from the interface to the surrounding medium. Coupled mass and heat transport are present in processes such as humidification of air and drying of solids [2], [3].

In all evaporation systems, it is necessary to have a good prediction and control of evaporation rate as a function of various system parameters [4]. In 1997, Eames et al, presented an equation determining the phase change rate as a function of the molecular weight and the interfacial temperature [5]. The evaporation characteristics of water droplets placed on three different hydrophobic surfaces was investigated in 2012 by Young Lee, it was found that the surface structure determines the motion of the contact line on the surface, which strongly influences the droplet evaporation characteristics [6].

Recently, computational fluid dynamics (CFD) simulation of evaporation process was studied showing that CFD is a powerful tool for simulation of simultaneous processes taking place within [7]. But in fact little work has been trying to review Psychrometry applied in practice.

Modeling and simulation of air-water direct contact process could be useful for illustrating the basic concepts for advanced contact mechanisms as in “membrane distillation” processes. However, modeling of such phenomena is not easy because both mass and heat transfer must be taken into account. A 2-D configuration of sweeping air over a flat water surface module is used. The basic equations including momentum, heat, and mass transfer are solved using CFD techniques.

2. Mathematical Modeling

Illustrated in figure 1, the lower domain represents the feed water, and the upper domain represents the air stream. The water is evaporated at the water–air interface, transported by diffusion through air molecules, and swept by the air stream out of the module. The approach used here neglects volume change of the water inside the module. Temperature difference between two phases is the driving force for transport of water.

The geometry and nominal conditions in the present study are as follows:
a) Air inlet boundary (A–C) and air outlet boundary (B–D): 45 mm
b) Lower vessel depth (C-E): 17 mm
c) Contact length for transportation process (C–D): 3.34m

e) Air velocity 1.71 m/s; total pressure 1 atm.; water temperature 25°C (as ambient); inlet air temperature 33.6°C (as ambient); inlet relative humidity 48%. One or more characteristics may be changed to reflect the system responses to these changes, but the others are kept unchanged.

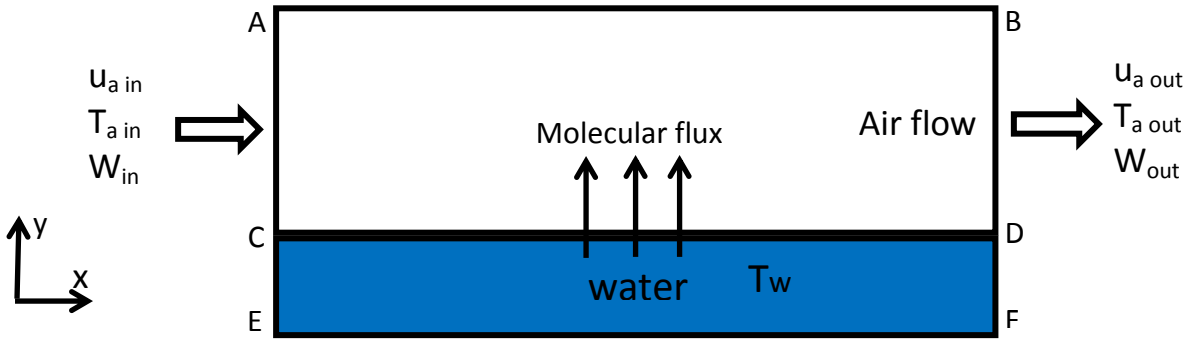

Fig. 1. Schematic of the Model Used in Simulation of the Present 2-D Study

2.1 Governing equations

2.1.1 Momentum

In air side, the compressible Navier-Stokes equations account for conservation of momentum and the continuity equation for conservation of mass in terms of air pressure and velocity vector in x-direction:

$$\rho_a \left[u_a\left(\frac{\partial u}{\partial x}\right)+v_a\left(\frac{\partial u}{\partial y}\right)\right]= - \frac{\partial}{\partial x}P+ \mu_a\left(\frac{\partial^2 u}{\partial x^2}+\frac{\partial^2 u}{\partial y^2}\right) \quad (1)$$

$$\left[\frac{\partial}{\partial x}(\rho u)+\frac{\partial}{\partial y}(\rho u)\right]_a = 0 \quad (2)$$

where ρ_a and μ_a are the density and dynamic viscosity of air, respectively. Turbulence effects are considered and modeled using the standard two-equation *k*-ε model because the Reynolds number is about 8×10^3. Assuming the velocity and pressure field is independent of the air temperature and moisture content. This allows calculating the turbulent flow field in advance and then using it as input for the heat and mass transfer species equations.

2.1.2 Heat transfer

In water side, the temperature is assumed constant all over the domain.
For air side, heat is transferred by convection and conduction mechanisms and the energy balance can be derived in terms of temperature and velocity vector of air in x-direction as:

$$\rho_a C_{pa} u_a\frac{\partial T_a}{\partial x} - k_a\left(\frac{\partial^2 T_a}{\partial x^2}+\frac{\partial^2 T_a}{\partial y^2}\right) = 0 \quad (3)$$

where ρ_a, C_{pa}, and k_a are the density (kg/m^3), specific heat capacity at constant pressure (J/kg.K), and thermal conductivity (W/m.K) of air, respectively.
The wet bulb temperature is determined by the given below equation (4) in the numerical model [8]:

$$T_{wb}= T\text{atan}[0.151977(\phi\%+8.313659)^{0.5}] + \text{atan}(T+\phi\%) - \text{atan}(\phi\%-1.676331) + 0.00391838(\phi\%)^{1.5}\text{atan}(0.023101\phi\%) - 4.686035 \quad (4)$$

2.1.3 Mass transfer

Transport of water vapor through the air is modeled by solving concentration equation considering the convection effect of the air stream beside the diffusional mass transfer. Concentration equation is a simplified form of continuity equation, and may be expressed as:

$$\nabla\cdot(-D\,\nabla c) + u_a \,.\, \nabla c = 0 \tag{5}$$

$$\frac{\partial}{\partial x}\left(-D\frac{\partial c}{\partial x}\right) + \frac{\partial}{\partial y}\left(-D\frac{\partial c}{\partial y}\right) + u_a\frac{\partial c}{\partial x} + v_a\frac{\partial c}{\partial y} = 0 \tag{6}$$

where c denotes the concentration of water vapor (mol/m^3) and D denotes the molecular diffusion coefficient of water vapor into air (m^2/s) estimated as [9]:

$$PD = 1.895\times10^{-5}\, T_w^{2.072} \tag{7}$$

where P is the total pressure (Pa), D in (m^2/s), and T_w is the water temperature (K).
The concentration at the water surface is given by the ideal gas law at saturation pressure:

$$c_w = \frac{P_{sat}}{R.T_w} \tag{8}$$

and the concentration at the air inlet boundary is calculated as:

$$c_0 = \frac{\phi_{in}.P_{sat}}{R.T_w} \tag{9}$$

where P_{sat} represents the pressure of saturated vapor at water temperature.
The water-vapor pressure at the water surface, P_{sat}, can be written with the Antoine equation [10, 11]:

$$P_{sat} = \exp\left(18.3036 - 3816.44/\left(T_w - 46.13\right)\right) \tag{10}$$

2.2 Numerical Solution of Governing Equations

The model equations relating momentum, heat, and mass transfer with the boundary conditions were solved using COMSOL Multiphysics® software with the help of its structure in estimating other properties and keeping the boundary and operating conditions as ranges. The package uses finite element method analysis and a mesh consisting of 53013 elements for numerical solution of the governing equations developed in this work. A system with the specifications of Intel® Core TM i5-4210U CPU @ 2.40 GHz and 6 GB RAM was used to solve the equations.

3. Experimental Work

The experimental device used can be seen in figure 2. The main part consists of a transparent 3 mm-Acrylic box with cross section 80 cm × 32 cm and height 60 cm representing the humidifier. The feed water is laid in six steel trays stacked inside the humidifier and having an apparent area of 0.1635 m^2 for each. This construction facilitates different configurations; packing, membranes, and spray dispersers.

The air was driven by a fan through 117 cm air duct shaped from commercial 2mm sheet-iron then circulated tangentially to the water surface in zigzag passage. For simplification, the air path was simulated as one tray has an equivalent length to the six trays. The temperature of

water was measured in third and last trays by probes NiCr/NiAl K-type connected to *Pacer®* digital thermometers model PT-2100 range from -65°C to 1150°C.

The sweeping air state was defined at the inlet by measuring the dry and wet bulb temperatures by two mercury thermometers fixed at 3.3 cm above water surface. At the middle and outlet of air path, dry bulb temperature, dew point temperature, and relative humidity were measured using thermistor sensor for temperature measuring with accuracy ±0.4°C and thin-film capacitance sensor for humidity measurements with accuracy ±1.5%. The sensors are connected to two digital multimeters *Traceable® type model Universal 4080.* At the middle air path one of the multimeters is fixed 2 cm above water surface and the other is fixed about 1 cm above water surface at the end of air path. The air flow was maintained with a *System air* fan 63 W model K160M and the range of the air pressure was between 100 and 280 Pa. The air velocity was measured by a *Florite-B* velocity meter ranges from 0 to 5 m/s.

In order to minimize the energy losses to the surroundings, the trays and the humidifier body were thermally isolated. The required time till the steady state may be reduced by adjusting water temperature to be close to that of inlet air state. The readings identifying the air states were recorded every 15 minutes for 2 hours.

4. Results and Discussion

With the model, parametric studies can be done. One set of parameters and operating conditions was chosen, as mentioned above in modeling part, to investigate the performance of the fabricated apparatus numerically and experimentally. First, the results of the computational model were validated with the experimental results. Second, the results of the model were illustrated. The water and air temperatures, air velocity, and relative humidity are inputs of the model. The distribution of dry and wet bulb temperatures, relative humidity, humidity ratio, velocity and enthalpy all over the model can be determined.

To be comparable with the experimental settings mentioned before, the numerical results were plotted at the cut line shown in Fig. 3

Figures 4, 5, and 6 show the values of air temperature, relative humidity, and humidity ratio along the air-water contact length, respectively. As illustrated in figure 4, almost a complete matching between numerical and experimental values of dry bulb temperature can be seen but 1% deviation at the outlet value. Relative humidity, figure 5 shows deviations of 9% and 3% at the middle and outlet air path, respectively. Figure 6 shows deviations of 1% and 0.5% at the middle and outlet air path, respectively. The accordance between the experimental data and the model predictions is clear.

The wet bulb temperature along the air path is an essential parameter that characterizes the performance. This character is reflected in figure 7 which shows one of the conditions of the air washer devices; constancy of air wet bulb temperature especially after the first 50 cm from the contact length

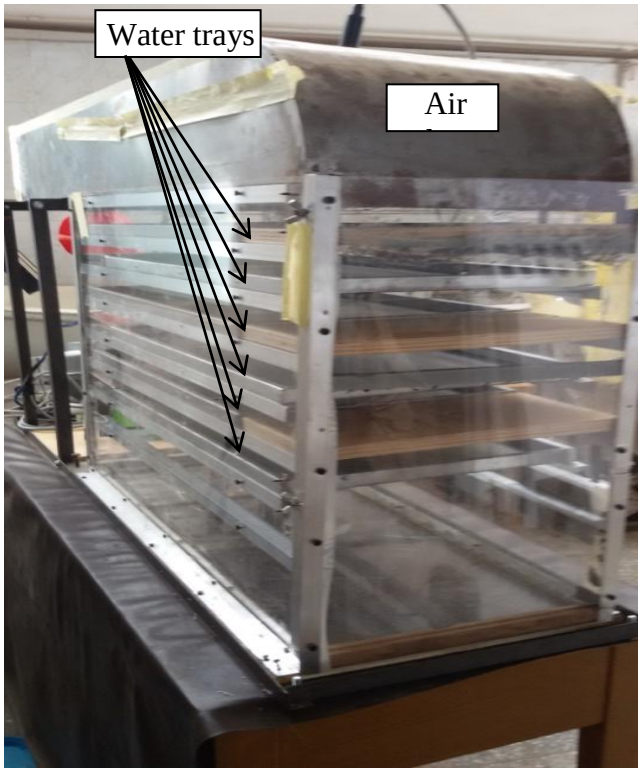

Fig. 2(a). Photo of the Experimental Setup

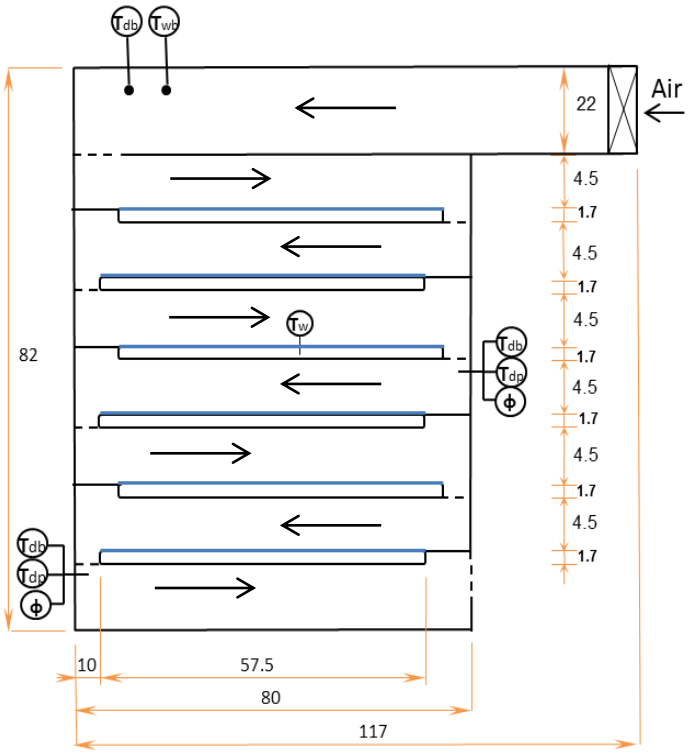

Fig. 2(b). Schematic of the Experimental Setup

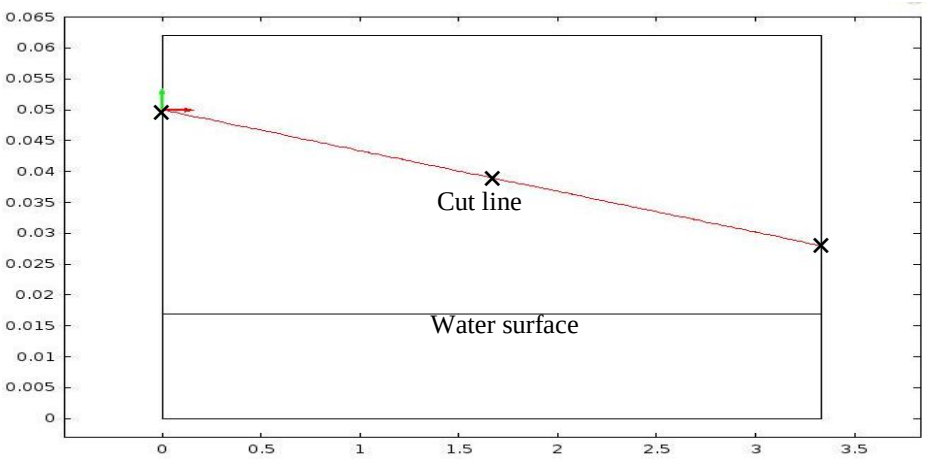

Fig. 3. Schematic of the 2-D Model Showing the Cut Line of Numerical Results

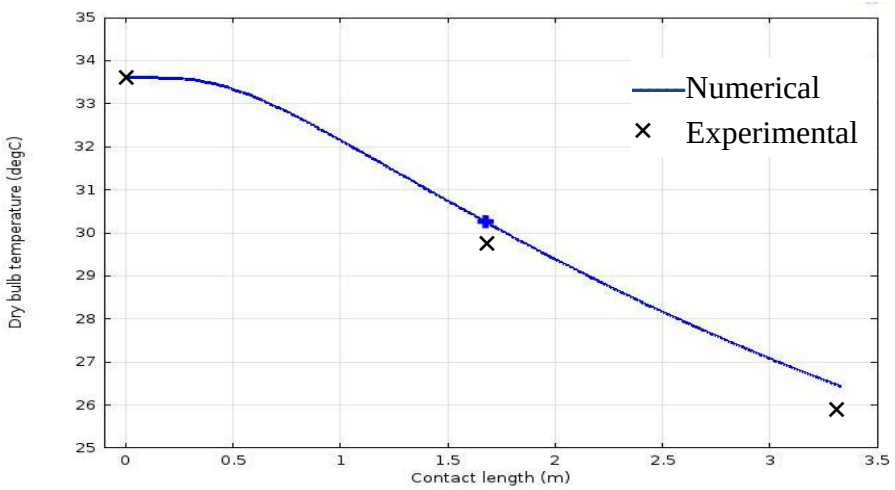

Fig. 4. Experimental and Numerical Dry Bulb Temperature vs. Contact Length

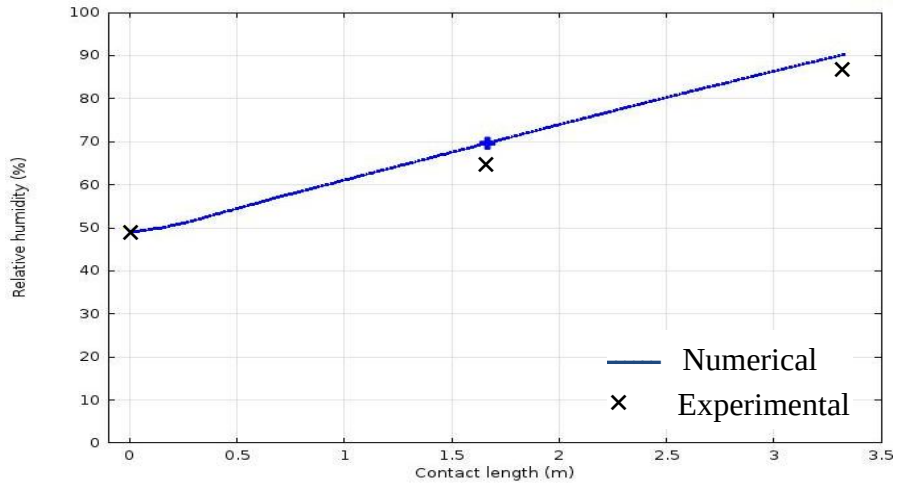

Fig. 5. Experimental and Numerical Relative Humidity vs. Contact Length

x

x

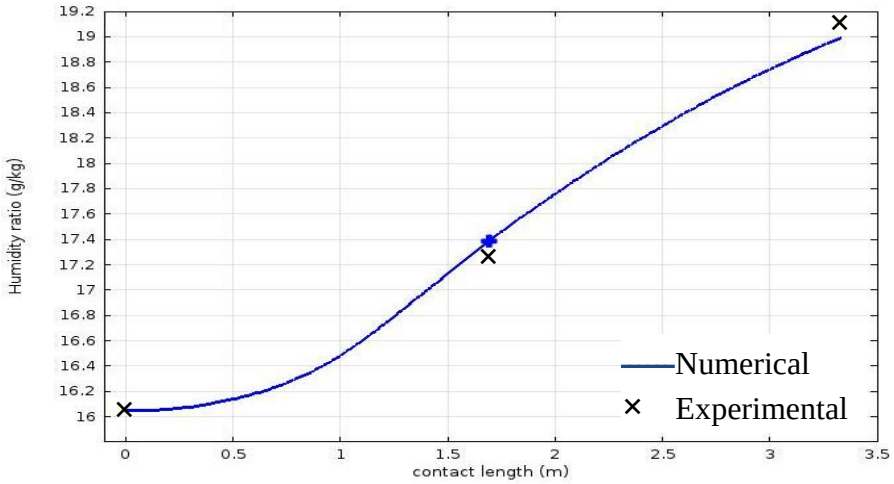

Fig. 6. Experimental and Numerical Humidity Ratio vs. Contact Length

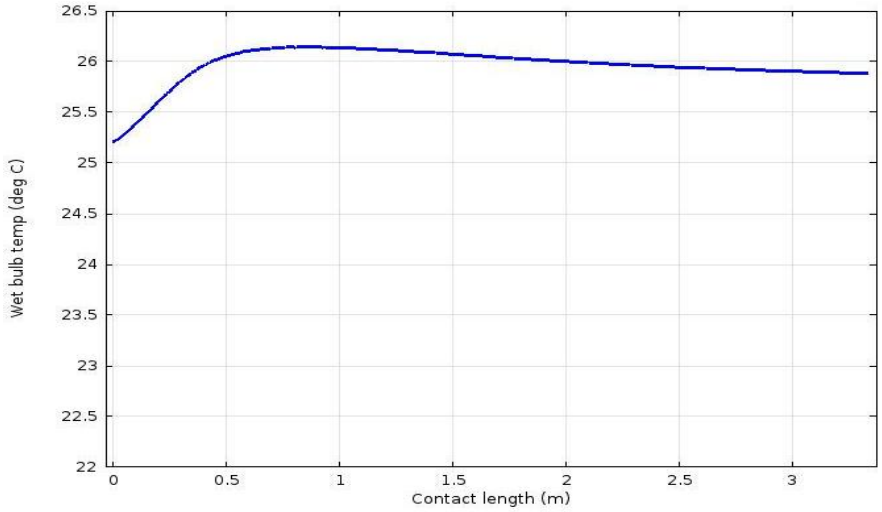

Fig. 7. Wet Bulb Temperature vs. Contact Length

The following figures show the results of the model according to our specified case. The temperature distribution is shown in figure 8. It is clear that the air temperature decreases gradually from air inlet temperature of 33.6°C to water surface temperature of 25°C in the area adjacent to the contact line. In respect of wet bulb temperature, figure 9 shows that almost all the values, except the entrance zone, fall in range between 25.4°C and 26.3°C with variation 3.4%. This trend is not unexpected if one considers that the device operated as an air washer.

By including the "*moist air*" thermodynamics in the numerical settings, both the relative humidity and humidity ratio distributions can be determined. The relative humidity distribution is illustrated in figure 10 which shows increase from 0.49 at air inlet boundary (as adjusted) till reach unity at water surface. Regarding to the humidity ratio, the average value

at air inlet can be calculated from the allowed information for air conditions to be 16.05 (g water vapor/ kg dry air)while the average value at the air outlet boundary is predicted as 18.5(g/kg) with increase of 15%, as illustrated in figure 11. This increase is expected due to the mass transfer by diffusion and convection from water into air. Also, it can be observed that the maximum humidity ratio is 20 g/kg at the layer adjacent to water surface which equals the moisture content for saturated air at defined water temperature (25°C).

As the upper and lower boundaries of air domain were considered as walls in the momentum modeling, the shown distribution for air velocity in figure 12 is normal. The air inlet velocity is 1.71 m/s which reaches to 1.93 m/s at the middle of air duct. Finally, figure 13 shows the enthalpy distribution which varies between 45.5 and 57.2 kJ/kg. The enthalpy increase can be considered as a direct outcome for the gradual increase of both dry bulb temperature and relative humidity.

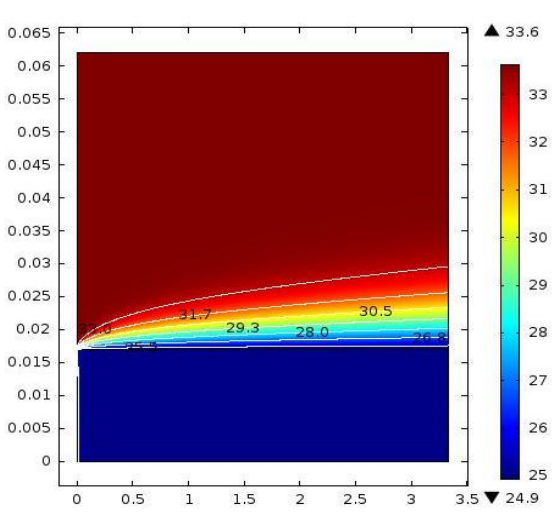

Fig. 8. Dry Bulb Temperature

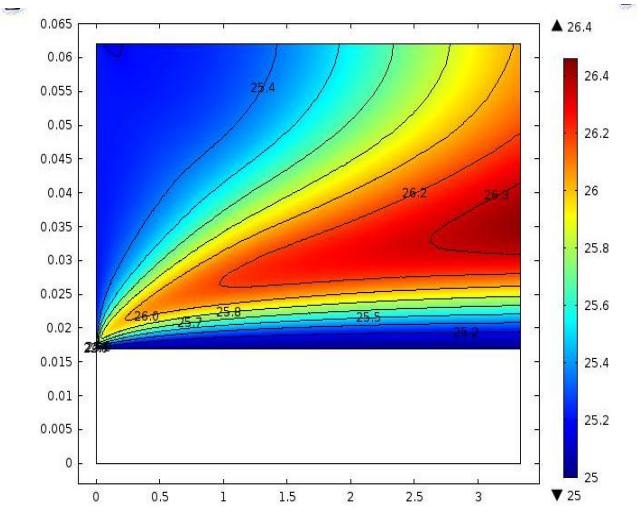

Fig. 9. Wet Bulb Temperature

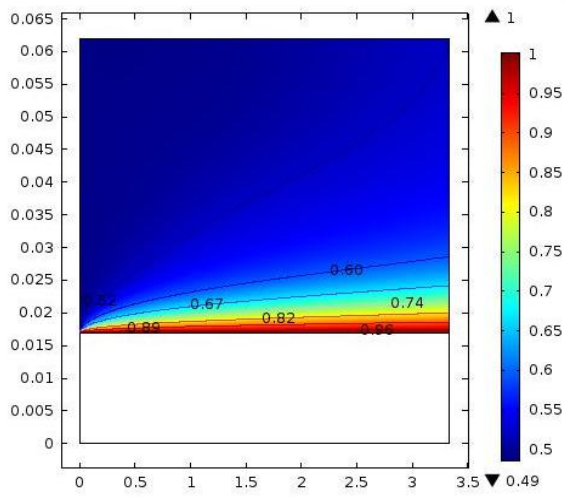

Fig. 10. Relative Humidity

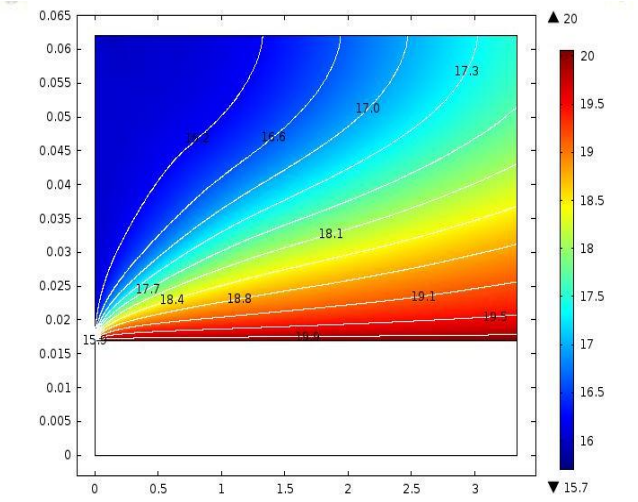

Fig. 11. Humidity Ratio (g/kg)

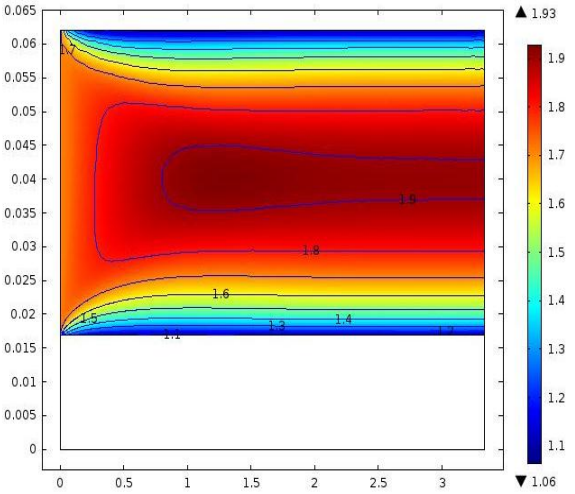

Fig. 12. Velocity (m/s)

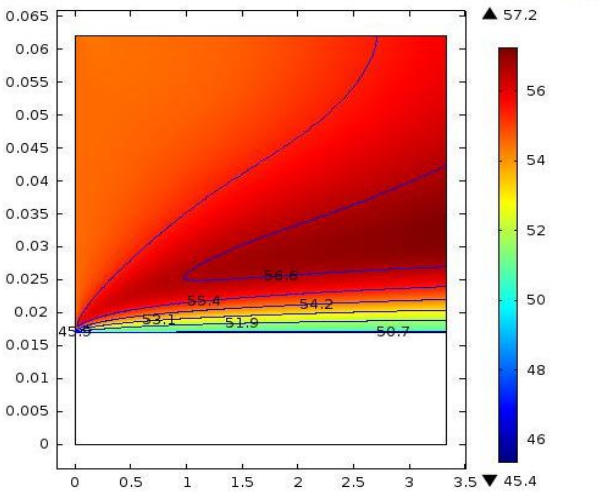

Fig. 13. Enthalpy (kJ/kg)

5. Conclusions

The model of direct contact air water system leading to heat and mass transfer in between has been rearranged in two-dimensional computational model considering the air as sweeping gas.

a) The CFD numerical simulation that was written to investigate the criterion of water transport in the previous model has proven consistence, when computational runs using COMSOL Multphysics® software were conducted. This software applies finite element method. Its results agreed well with analytical and experimental performance of an air washer humidifier.

b) The laboratory scale experimental humidifier aiming at obtaining flexible arrangement to investigate the performance of different configurations of air water interfacial area has performed well as an air washer.

c) It was thus concluded that further investigations of other humidification processes, through other interfacial configurations are possible, using that test rig and the built computational model.

6. References

[1] Matilda Lundberg, "Modeling & Simulation of a Cooling Tower with COMSOL Multiphysics", 2015, MSc thesis, Department of Chemical Engineering, Lund University.

[2] W. L. McCabe, J. Smith, and P. Harriott, Unit Operations of Chemical Engineering. 2005.

[3] S. Stenström, "Transportprocesser," in Industriella Seperations processer, Lund: Institutionen för kemiteknik, LTH, 2009, pp. 19–60.

[4] Zhi Huang, Yuanchen Hu, Kang Liu, and Xuejiao Hu, "Unusual Fast Evaporation From Nanoholes", ASME 2012 International Mechanical Engineering Congress & Exposition, 2012, IMECE2012-87147.

[5] Eames, I. W., Marr, N. J., and Sabir, H., "The evaporation coefficient of water: a review", International Journal of Heat and Mass Transfer, 1997, 40: 2963-2973.

[6] Chi Young Lee, Bong June Zhang, Jiyeon Park, and Kwang J. Kim, "Water droplet evaporation on Cu-based hydrophobic surfaces with nano and micro-structures", International Journal of Heat and Mass Transfer, 2012, 55: 2151-2159.

[7] COMSOL Multiphysics 5.2 Tutorials, Application Library path:

Heat_Transfer_Module/ Phase_Change/ evaporative_cooling.

[8] Roland Stull, "Wet-Bulb Temperature from Relative Humidity and Air Temperature", Journal of Applied Meteorology and Climatology, 2011, 50: 2267-2269, DOI: 10.1175/JAMC-D-11-0143.1.

[9] Abdullah Alkhudhiri, Naif Darwish, and Nidal Hilal, "Membrane distillation: A comprehensive review", Desalination, 2012, 287: 2–18, DOI:10.1016/j.desal.2011.08.027.

[10] K. W. Lawson and D. R. Lloyd, "Membrane distillation", J. Membr. Sci., 1997, 124 (1), 1−25.

[11] Efrem Curcio and Enrico Drioli, "Membrane Distillation and Related Operations—A Review", Separation and Purification Reviews, 2005, 34: 35–86, DOI: 10.1081/SPM-200054951.

[12] I. Hitsov, T. Maere, K. De Sitter, C. Dotremont, and I. Nopens, "Modelling approaches in membrane distillation: A critical review", Separation and Purification Technology, 2015, 142: 48–64, DOI:10.1016/j.seppur.2014.12.026.